Improvement of the Gerchberg-Saxton Algorithm Convergence in Phaseless Antenna Measurements via Spherical-Wave Filtering

Nicolas Mezieres, Laurent Le Coq

Improvement of the Gerchberg-Saxton Algorithm Convergence in Phaseless Antenna Measurements via Spherical Wave Filtering

Nicolas Mézières and Laurent Le Coq

***Abstract*—The phaseless characterization of antennas enables configurations with reduced measurement efforts as the phase acquisition is highly sensitive to numerous error sources. However, both the magnitude and phase information are necessary to reconstruct the 3D radiation pattern of the tested radiating system. The two scans technique allows for accurate phase retrievals from magnitude-only measurements. In this paper, the two concentric spheres setup is considered with a Gerchberg-Saxton (GS) algorithm as phase retrieval procedure. These methods are known for their convergence problems, the price to pay for the easier, magnitude-only, measurements. A filtering approach is studied to mitigate these effects and a new, more efficient, filter is proposed. A loop of GS runs coupled with filters is shown to improve the radiation pattern reconstruction without much considerations. Validations are led on simulations and experimental data acquired using a commercial system.**

***Index Terms*—Antenna measurements, near field, phaseless measurement, phase retrieval, spherical waves.**

I. Introduction

THE characterization of antennas using spherical Near-Field (NF) measurements is a standard procedure in antenna prototyping and development enabling the reconstruction of the 3D radiated field. The ever-growing complexity of radiating systems has led to numerous and mandatory developments of post-processing strategies. Many of them are dedicated to spherical measurements with Spherical Waves (SW) [1], including phaseless measurements, that aims at avoiding the complex phase evaluation task thanks to appropriate samplings and processing methods. However, the phase information is mandatory for the full radiation pattern to be reconstructed. As a counterpart of the simplified measurements, the data processing is tedious since phase retrieval problems are often ill-conditioned, as emphasized in [2].

Various phase retrieval approaches for antenna measurements are available, as reviewed in [3]. The most spread phaseless antenna characterization method is the two scan technique. The field is sampled over two measurement surfaces with various geometries or/and a priori information on the Antenna Under Test (AUT) [3]–[5]. These surfaces might be concentric spheres [6] (cf Fig. 1), two planes [7] or even a combination of a plane and a sphere [8]. A single sphere but for two positions of the AUT has been proposed and validated in [9], [10]. Others methods with different probes or interferometric methods are studied in [11], [12], respectively.

Manuscript received xx, 2022; revised xx, xx.

This work is supported in part by the European Union through the European Regional Development Fund (ERDF), and by the french region of Brittany, Ministry of Higher Education and Research, Rennes Métropole and Conseil Départemental 35, through the CPER Project SOPHIE / & STIC Ondes.

N. Mézières and L. Le Coq are with IETR (e-mail: nicolas.mezieres@univ-rennes1.fr) ,UMR CNRS, Rennes, France.

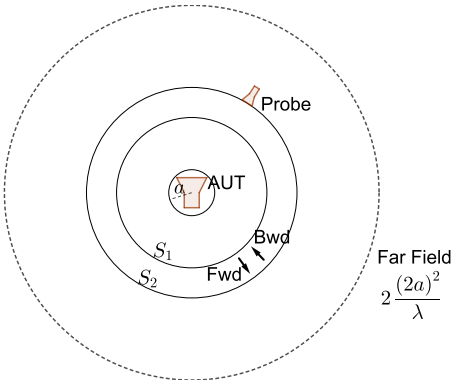

Fig. 1. Scheme of a two scan method with NF spheres S_1, S_2. In a given coordinate system, the radiated field possesses a unique SW expansion outside the minimum sphere (whose center coincides with the origin), of radius a.

The present article focuses on two concentric spherical scans combined with a Gerchberg-Saxton (GS) algorithm. Such method possesses the interesting property to be computationally efficient and to converge systematically, but often to local minima, as reported in [6]. This paper has studied the possible configurations (in term of sampling ratios, distributions and sphere radii) leading to successful phase retrieval using the GS algorithm. The numerous minima may be avoided by using a quadratic inversion approach, as investigated in [2], [13], but it requires more scans. Finally, a filtering approach has been proposed in [14] to clear out the high degree spherical waves above a given index. A new filter is proposed here and compared to this one. Several initialization methods are used for completeness. Interestingly, these filters can be applied directly on many phase retrieval algorithms with SW expansion, for example with convex optimization [7], [15], as soon as phase initialization is possible.

The paper is organized as follows. The SW expansion and the used GS algorithm are defined in Section II. The filtering approach is described in Section III. Validations on simulations and experimental data are shown and discussed in Section IV. Finally, conclusions are drawn in Section V.

II. Phaseless Spherical Near-Field Measurement

A. Spherical Wave Expansion

The electric field $\mathbf{E}$ radiated from sources can be expanded outside the minimum sphere enclosing them using Spherical Waves (SW) $\mathbf{F}_{smn}$ as follows [1]

$$\mathbf{E}(r,\theta,\varphi) = \frac{k}{\sqrt{\eta}} \sum_{smn} Q_{smn} \mathbf{F}_{smn}(r,\theta,\varphi) \qquad (1)$$

where k is the wavenumber, η the admittance of the propagation medium and (r,θ,φ) the spherical coordinates. The

quantities Q_{smn} are the complex coefficients to be determined. The series (1) is truncated to $n \leq N$ according to the rule $N = \lfloor ka \rfloor + n_1$ where a is radius of the minimum sphere, $\lfloor x \rfloor$ the floor function and n_1 an integer [1], set to 10 [16]. If the electric field radiated by the AUT is sampled at M positions, the SW expansion of the field (1) can be rewritten as a linear system of equations

$$\mathbf{y} = \mathbf{A}\mathbf{x} \tag{2}$$

where the vector $\mathbf{y}$ of size $2M$ gathers the complex measured field (two polarizations), $\mathbf{A}$ is the matrix containing the SW, $\mathbf{F}_{smn}$, at the sampling positions and $\mathbf{x}$ stores the spherical coefficients Q_{smn}. The linear system (2) can be solved in the least-square sense by computing the pseudo-inverse of $\mathbf{A}$. The solution is given by $\mathbf{x} := \widetilde{\mathbf{A}}^{+}\widetilde{\mathbf{y}}$ where the matrix $\widetilde{\mathbf{A}}^{+}$ is the pseudo-inverse of $\mathbf{A}$ with controlled conditioning. Such task is achieved by an appropriate truncation of the singular value decomposition.

B. Gerchberg-Saxton Algorithm

The GS algorithm for spherical antenna measurements propagates the complex field back and forth between the two sampled NF spheres, S_1, S_2 in Fig. 1, until convergence of the SW expansion. The fields share the same spherical coefficients Q_{smn} over both spheres, allowing for the field propagation. After such operation, the magnitude is replaced by the measurement data but the propagated phase is kept. This process goes on until some stopping criterion is satisfied. In the sequel, this criterion is defined to be a minimum change occurring between two iterations. A maximum iteration count $\max_{iter}$ is set to avoid unwanted, extended, computations. The implementation is detailed in Algo. 1.

Algorithm 1 Gerchberg-Saxton for phaseless measurements

Require: $|\mathbf{y}_1|, |\mathbf{y}_2|$ the measured magnitudes, $\mathbf{A}_1, \mathbf{A}_2$ the SW matrices for the two measurement spheres S_1, S_2 and their pseudo-inverses $\widetilde{\mathbf{A}}_1^{+}, \widetilde{\mathbf{A}}_2^{+}$, $\phi^{(0)}$ a starting phase guess, tol the minimum required change, $\max_{iter}$ the maximal number of iterations.

1: **Initialization**
2: $\widetilde{\mathbf{y}}_1 \leftarrow |\mathbf{y}_1| e^{i\phi^{(0)}}$ #Assign starting phase
3: $\widetilde{\mathbf{y}}_1^{(-)}, \leftarrow \widetilde{\mathbf{y}}_1, \varepsilon = tol$ #For stopping criterion
4: $iter \leftarrow 0$ #Iteration count
5: **while** $\varepsilon \geq tol$ and $iter < \max_{iter}$ **do**
6: $\quad \mathbf{x} \leftarrow \widetilde{\mathbf{A}}_1^{+}\widetilde{\mathbf{y}_1}$ #Solving for the coefficients on S_1
7: $\quad \widetilde{\mathbf{y}}_2 \leftarrow \mathbf{A}_2\mathbf{x}$ #Propagate to S_2
8: $\quad \boldsymbol{\phi}_2 \leftarrow \text{Phase}(\widetilde{\mathbf{y}}_2)$ #Store the retrieved phase
9: $\quad \widetilde{\mathbf{y}}_2 \leftarrow |\mathbf{y}_2| e^{i\boldsymbol{\phi}_2}$ #Magnitude correction
10: $\quad \mathbf{x} \leftarrow \widetilde{\mathbf{A}}_2^{+}\widetilde{\mathbf{y}}_2$ #Solving for the coefficients on S_2
11: $\quad \widetilde{\mathbf{y}}_1 \leftarrow \mathbf{A}_1\mathbf{x}$ #Propagate to S_1
12: $\quad \boldsymbol{\phi}_1 \leftarrow \text{Phase}(\widetilde{\mathbf{y}_1})$ #Store the retrieved phase
13: $\quad \widetilde{\mathbf{y}}_1 \leftarrow |\mathbf{y}_1| e^{i\boldsymbol{\phi}_1}$ #Magnitude correction
14: $\quad \varepsilon \leftarrow \|\widetilde{\mathbf{y}}_1^{(-)} - \widetilde{\mathbf{y}}_1\|$ #Evaluate change norm
15: $\quad \widetilde{\mathbf{y}}_1^{(-)} \leftarrow \widetilde{\mathbf{y}}_1$ #Store to evaluate change
16: $\quad iter \leftarrow iter + 1$ #Iteration count update
17: **return** $\mathbf{x}$ #Complex spherical coefficients

The evaluation of the coefficients in $\mathbf{x}$ and field propagation are performed by a matrix-vector multiplication. The pseudo-inverses $\widetilde{\mathbf{A}}_1^{+}, \widetilde{\mathbf{A}}_2^{+}$ are costly to evaluate, especially for large systems, but contain most of the complexity of the procedure. Therefore, once computed, large iteration counts $\max_{iter}$ and/or several runs with different phase initialization are possible within reasonable computation times.

C. Phase Initialization

The GS algorithm requires a starting phase, $\phi^{(0)}$. The used methods do not require *a priori* information on the AUT. Three methods are used for benchmark purposes.

1) Constant phase: The starting phase is $\phi^{(0)} = 0$ (or any real constant), noted as 0-Pha thereafter. It is highly non-physical but provides the most simple, unbiased, choice.

2) Dipole phase: The phase $\phi^{(0)}$ is taken from an Hertzian dipole, noted as Dip.Pha. The direction of the dipole is chosen to avoid phase jumps at high magnitude positions, as in [6].

3) Correlated SW Phases: The phase is provided by a set of randomly drawn coefficients using low-degree SW with the highest correlation relatively to the input magnitude data, denoted by Corr.Q in the sequel. It generates more complex starting phases with no jumps at high magnitude levels.

III. Filtered Gerchberg-Saxton

The GS algorithm is simple but its convergence is slow and often trapped in local minima [6]. To mitigate these effects, a filter procedure is used. A new GS run is initialized with the previously found phase to which a filter has been applied. The resulting algorithm is named Filtered GS (FiGS) in this paper.

A. Principle

At the end of the GS run (either by hitting tolerance tol or maximal number of iterations $\max_{iter}$), a filter is performed on the retrieved complex spherical coefficients $\mathbf{x}$. The filtered coefficients yield a phase pattern for a new GS run. The proposed filters aim to clear the aliasing on high-degree SW introduced during minimization, as noted in [14] and illustrated in Section III-B3. Conversely, the filters must not enforce specific distributions of the SW coefficients but only guide the convergence of the GS algorithms. Hence, the filters attenuate as detailed in Section IV-B2. An alternative approach would be to apply the filters within the GS algorithm, between lines 6-7 and 10-11 in Algo. 1. However, as the GS technique is equivalent to a Steepest-Descent algorithm [17], such method would produce a perturbed descent leading to worse performances results as confirmed by several tests (not shown here for conciseness) relatively to the proposed implementation (in stability, accuracy and speed of convergence). This method is thus left aside for this paper.

B. Filter methods

1) n-Low-Pass Filter (n-LPF): A low-pass filter whose cutoff is a maximal degree n_T given by a chosen percentage of the total radiated power [14]. The index n_T corresponds to the first degree such that $P\%$ of the total radiated power is radiated. This filter sets to 0 every spherical coefficients Q_{smn} with degree $n > n_T$.

This article has been accepted for publication in IEEE Transactions on Antennas and Propagation. This is the author's version which has not been fully edited and content may change prior to final publication. Citation information: DOI 10.1109/TAP.2023.3249355

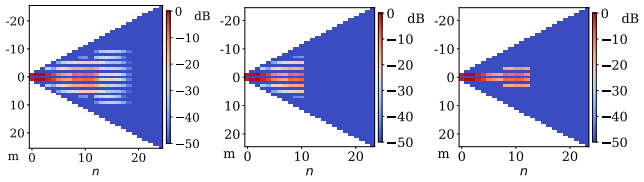

(a) No Filter (b) n-LPF (c) nm-MT

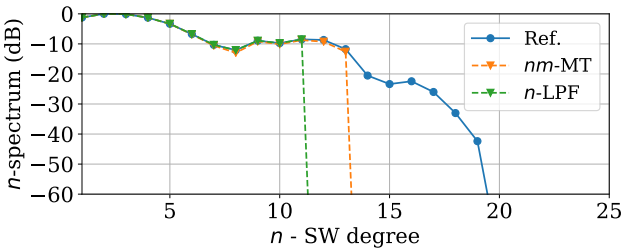

(d) n-spectra of the coefficients displayed in Fig. 2

Fig. 2. Simulated horn antenna: effects of the filters on the SW coefficients for $P = \alpha = 99\%$. The corresponding n-spectra are shown in (d).

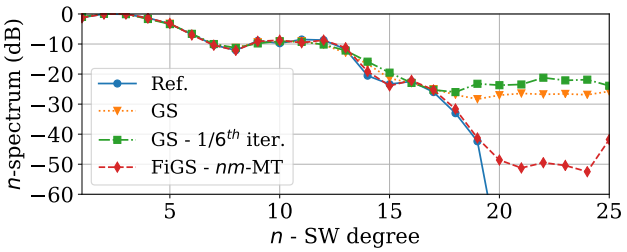

Fig. 3. Simulated horn antenna: n-spectra after a run of GS, before the first filtering operation and at the end of FiGS for the nm-MT filter.

2) nm-Maximum-Threshold (nm-MT): A riddling of the least contributing coefficients over both the degree n and the order m, introduced by this paper. A threshold α determines the dynamic over the normalized SW expansion coefficients $Q_{smn}/\max|Q_{smn}|$. As a result, the spherical coefficients in $\mathbf{x}$ with magnitude less than $(1-\alpha)\max_j|\mathbf{x}_j|^2$ are set to 0.

3) Observations and illustrations: The effects of both filters are showcased in Fig. 2 on a simulated horn antenna in X band. The spectra for $s = 1$ are shown in Fig. 2.a,b,c and the distribution of the radiation power over the degrees, the n-spectrum, in Fig. 2.d. The n-spectrum is the sum of powers radiated by the modes of degree n. The tail of the distribution is cut abruptly as it contains small magnitudes only. Intuitively, the filters clear out the fast but small oscillations to provide a new starting phase. As illustrated by the n-spectra in Fig. 3, at one sixth of the maximal number of iterations (before the first filter), the solution contains many high degree modes $n \geq 20$. These modes are not present in the true set of coefficients and the power distribution is not modified significantly thereafter by the GS algorithms as compared to the FiGS run.

IV. Numerical and Experimental Validations

A. Characterization Accuracy

The success of the phaseless characterization is evaluated by comparing the retrieved Far Field (FF) in $\widetilde{\mathbf{y}}$ from the phaseless NF data to the reference one, $\mathbf{y}$. This comparison is achieved point-wise by the error signal defined as follows

$$\text{Error}(\mathbf{y},\widetilde{\mathbf{y}}) = \frac{||\mathbf{y}| - |\widetilde{\mathbf{y}}||}{\max_i |\mathbf{y}_i|}. \tag{3}$$

The mean of this error signal is the Equivalent Noise Level (ENL). Both are given in dB. The comparison of the FF magnitudes provides a single, straightforward, indicator of a coherent retrieved phase in NF as faithful FF reconstruction is not possible otherwise. It also avoids the comparison of phase patterns, which is tedious for phase reference reasons.

B. Methodology

1) Phaseless configuration: The NF spherical samplings use the *igloo* strategy [18] as it provides a somewhat uniform sampling distribution, as advised in [15]. The coordinate system are the ones used for the simulation or the one of the MVG StarLab [19] for the measurements. The distance is evaluated as a % of the FF distance given by the Rayleigh definition, $r_{FF} = 2\frac{(2a)^2}{\lambda}$. The sampling ratio δ is the number of data on each sphere over the number of unknowns. The total sampling ratio is 2δ as two scans are performed. The NF sphere radii are chosen according to [6]. The FF cutting planes are shown for $|\theta| \leq 135°$ for readability and results from the phase initialization having the best FF reconstructions. The ENL metrics are however computed on the whole spheres.

2) Filter implementation and algorithm comparison: The filters are designed to guide the convergence of the GS algorithm but not to enforce the solution. Consequently, the successive filtering operations attenuate. In this paper, it translates into the following: a starting threshold α_0 or P_0 is chosen and increases linearly toward 99.9%. For example, if the starting value is $\alpha_0 = 90\%$ and the filter is applied 3 times, the thresholds are respectively $90, 94.95$ and 99.9%. Also, the maximal number of iterations between two filtering operations is fixed and chosen so the maximal total iteration count is the same for the GS and FiGS algorithms. Finally, the tolerance parameter is set to $tol = 10^{-6}$. These choices are empirical and help avoiding unfair comparisons due to prematurely stopped algorithms.

3) Filter tuning: For each filter, the starting threshold α_0/P_0 and the number of filtering have to be set. Extensive testings for a wide range of possible values have been performed on the presented cases to demonstrate the stability. In particular, the tests for the simulated horn antenna are provided in section IV-C1 and show similar behaviors for the other antennas. Consequently, for all cases, the n-LPF filter is applied 1 times with threshold $P = P_0 = 95\%$ and the nm-MT filter 5 times with thresholds α increasing linearly from $\alpha_0 = 99\%$ to 99.9%, as motivated in Section IV-D2. For a total maximal iteration of 2000 in both simulation cases, the n-LPF filter is applied at most at the 1000th iteration and the nm-MT one at most every 333 iterations. If minimum tolerance tol is reached before, the next filter, if performed, occurs earlier.

C. Simulations

Two antennas are considered; a model of the horn antenna in X band in Fig. 9 and a 5×5 array of rectangular wave-guides

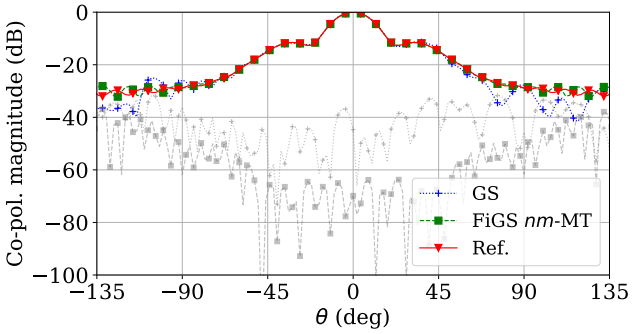

(a) Co-polarization

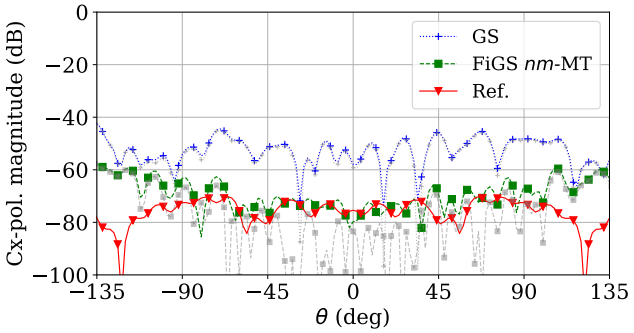

(b) Cross-polarization

Fig. 4. Simulated horn antenna: reconstructions of the FF in the E-plane using GS and FiGS with the proposed nm-MT filter. Error signals relatively to reference are in grey with same style as their parent curve.

(WG array) at 30 GHz with a tilted main beam, providing two very different patterns. The simulations are performed on CST [20] and data exported on NF and FF spheres. The ENL values between the FF reconstruction from the phaseless data and the reference FF are given in Table I. The total maximal number of iterations is set to $\max_{iter} = 2000$ for both cases.

1) Horn antenna at 10 GHz*:* This antenna has a minimum sphere radius $a = 75\,\text{mm}$, $N = 25$. The two NF spheres S_1 and S_2 are located at 150 and 225 mm, or 10 and 15 % of the FF distance, respectively. There are 2744 samples for each sphere and 1350 coefficients to identify (sampling ratio $\delta \approx 2.03$). The reconstructions of FF co- and cross-polarizations in the E-plane are shown in Fig. 4. The ENL of the reconstructions on S_1 over the iterations are shown in Fig. 5, illustrating the effects of the filter on the convergence. The ENL of FF reconstructions relatively to the sampling size (sampling ratio) and to filter tuning are shown in Fig. 6 and 7, respectively. These results are discussed in the next section.

2) Waveguide array at 30 GHz*:* The array has a minimum sphere radius $a = 48\,\text{mm}$, $N = 40$. The NF spheres are located at 184 and 277 mm, or 10 and 15 % of the FF distance, respectively. There are 6832 samples for each sphere and 3360 coefficients to identify (sampling ratio $\delta \approx 2.03$). The reconstructions of the co-polarization of the FF in two orthogonal places going through the maximum at $(\theta, \varphi) = (30°,290°)$ are shown in Fig. 8.

D. Discussions on Simulations

1) Accuracy of the FF: According to Table I, the FiGS algorithm produced more accurate results in all cases. This

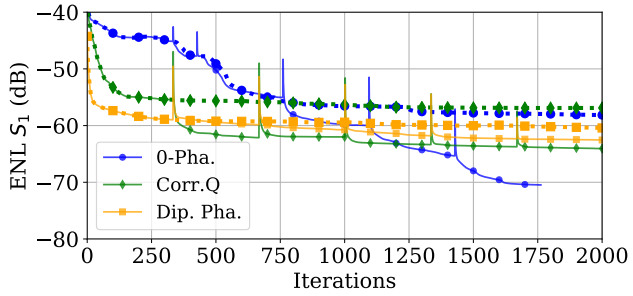

Fig. 5. Simulated horn antenna: ENL of the reconstructions on the first measurement sphere S_1 during a run of GS (dotted curves) and FiGS (plain curves) with nm-MT filter.

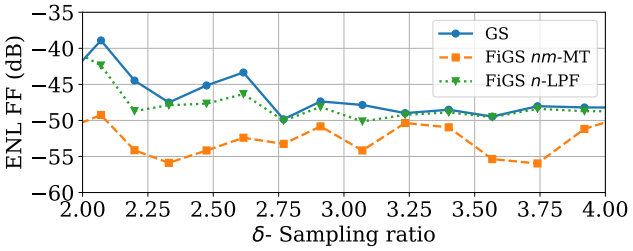

Fig. 6. Simulated horn antenna: ENL of the FF reconstructions error relatively to the sampling ratio.

TABLE I
SIMULATIONS : FF RECONSTRUCTION PERFORMANCES IN ENL

Horn	0-Pha	Dip.Pha	Corr.Q
GS	-44.0	-47.6	-47.4
FiGS n-LPF	-48.7	-47.7	-48.2
FiGS nm-MT	-55.1	-50.1	-52.5
WG array	0-Pha	Dip.Pha	Corr.Q
GS	-41.5	-42.1	-41.9
FiGS n-LPF	-42.2	-43.3	-42.6
FiGS nm-MT	-45.5	-45.7	-45.1

observation is further illustrated in Fig. 6 for various dataset sizes. Finally, the proposed nm-MT filter yields significantly better results in a more stable way. A possible explanation is that the nm-MT filter also acts on the order m. Since there is a multiplicative term $e^{jm\varphi}$ in the SW expression, which has constant modulus, the order m is highly critical for phase ambiguities. The lower error signal in the various

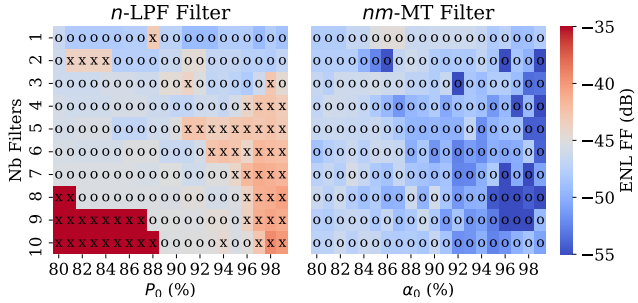

Fig. 7. Simulated horn antenna: ENL of the FF reconstruction with FiGS using both filters relatively to the number of filtering operations and the starting threshold. For each choice, markers 'o' and 'x' mean that ENL has been improved or deteriorated, respectively.

This article has been accepted for publication in IEEE Transactions on Antennas and Propagation. This is the author's version which has not been fully edited and content may change prior to final publication. Citation information: DOI 10.1109/TAP.2023.3249355

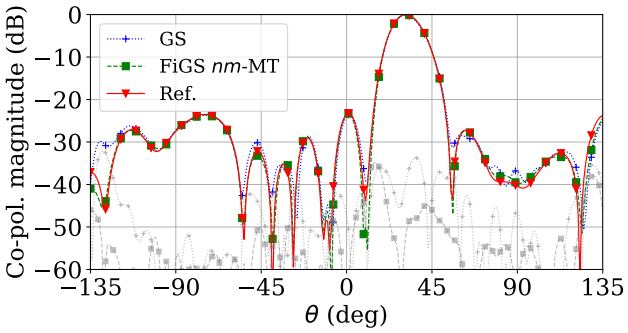

(a) Principal plane ($\varphi = 290°$)

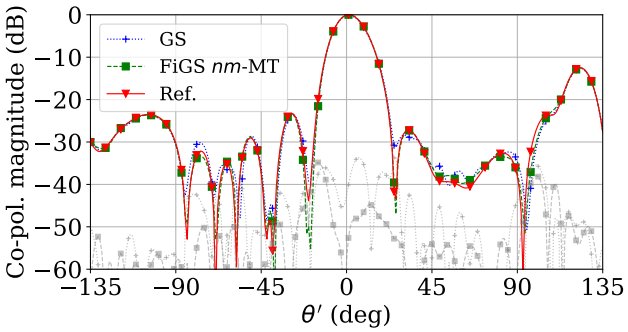

(b) Co-principal plane ($\theta' = 0$ indicates $(\theta, \varphi) = (30°,290°)$)

Fig. 8. Simulated WG array: reconstructions of the FF co-polarization in two orthogonal planes going through the maximum. The angle θ' represents the angle θ in the coordinate system pointing at the maximum. Error signals relatively to reference are in grey with same style as their parent curve.

cutting planes also illustrates the claimed improvements.

2) Choice of the parameters: The filtering approach relies on two parameters: the number of filters and the starting threshold α_0. Without a FF reference, a rule of thumb for the parameter tuning is to observe the achieved ENLs on the measurement spheres. Indeed, the final values of the FiGS curves in Fig. 5 follow the same order as the FF reconstruction accuracy in Table II. Note that one FiGS curve stops around 1750 because the minimum tolerance tol is reached. The filter operations are visible as spikes. The parametric studies reported in Fig. 7 motivate the set values for both filters as they lie in the region where the improvements are the most significant and stable. Similar behavior can be observed for the other AUTs (not shown here for conciseness), allowing the fixed values used throughout the paper. It also shows how more stable and efficient is the proposed nm-MT filter.

E. Data from Measurements

The NF measurements have been performed in the StarLab for the horn antenna previously simulated and a metasurface antenna [21]. The (complex) SW coefficients returned by the MVG software are used to generate the phaseless samplings. The ENL values between the FF reconstructions from the phaseless NF and the reference are given in Table II.

1) Horn antenna at $10\,\mathrm{GHz}$*:* The data parameters are the same as in the simulation except for the sampling distances, of 320 and $450\,\mathrm{mm}$ (the StarLab radius), or 20 and 30 $\%$ of the FF distance, respectively. The FF reconstructions of one polarization in two planes are shown in Fig. 10.

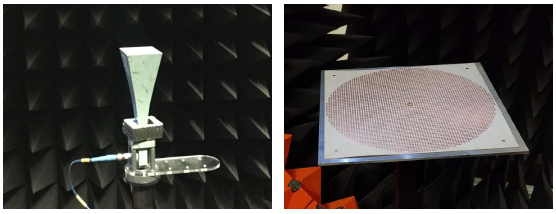

(a) Horn (b) Metasurface [21]

Fig. 9. Pictures of the antennas measured in the MVG Starlab for the experimental validations of the phaseless characterization procedure.

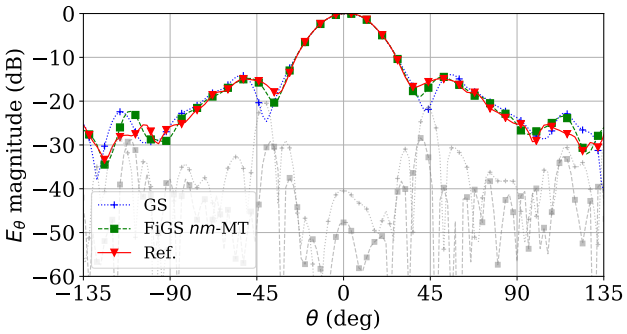

(a) E_θ in E-plane (Co-polarization)

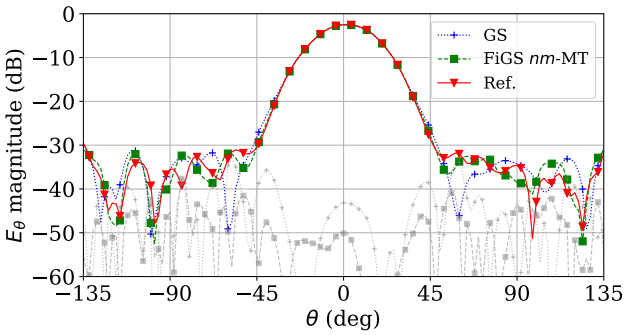

(b) E_θ in the plane $\varphi = 45°$

Fig. 10. Horn antenna: FF reconstructions of E_θ in two planes. Error signals relatively to reference are in grey with same style as their parent curve.

2) Metasurface antenna at $17\,\mathrm{GHz}$*:* This antenna has a minimum sphere radius $a = 130\,\mathrm{mm}$, $N = 56$. The two NF spheres are located at 450 and $900\,\mathrm{mm}$, or 6 and 11 $\%$ of the FF distance, respectively. There are 14264 samples for each sphere and 6496 coefficients to identify (sampling ratio $\delta \approx 2.20$). The maximal iteration count is $\max_{iter} = 3000$. Both larger sampling ratios and maximal iteration count are due to the high complexity of the antenna to ensure proper convergence of all the methods. The reconstructions of co- and cross-polarizations of the FF in the main cutting plane are shown in Fig. 11.

3) Summary and Usage Guidelines: The FiGS algorithm has led to improved accuracy of between 1.1 and $2.5\,\mathrm{dB}$ in mean and better side-lobes reconstructions using predetermined values, as shown by the ENL in Tab. II and displayed cutting planes. It has to be noted that the metasurface antenna is in circular polarization with two tilted main beams with low directivity, explaining the worse ENL levels despite the larger samplings and maximal iteration count. These studies allow the following conclusions: the nm-MT filter is more

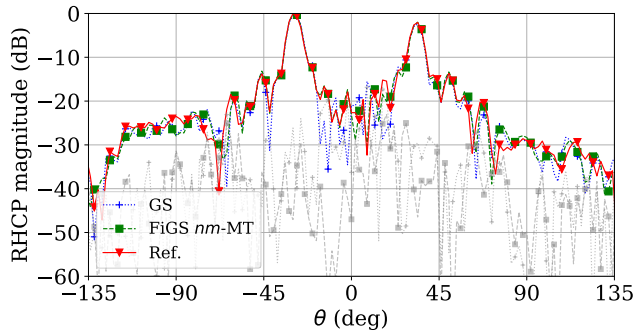

(a) RHCP (Co-polarization)

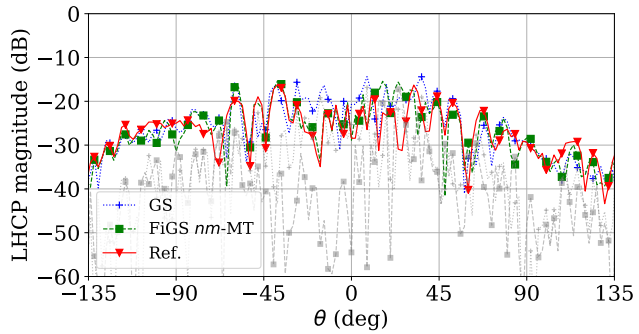

(b) LHCP (Cross-polarization)

Fig. 11. Metasurface antenna: FF reconstructions in the principal plane. Error signals relatively to reference are in grey with same style as their parent curve.

TABLE II
MEASUREMENTS : FF RECONSTRUCTION PERFORMANCES IN ENL

Horn	0-Pha	Dip.Pha	Corr.Q
GS	-42.0	-42.3	-42.1
FiGS n-LPF	-42.2	-42.6	-44.1
FiGS nm-MT	-43.8	-42.8	-44.6
Metasurface	0-Pha	Dip.Pha	Corr.Q
GS	-35.0	-35.2	-34.8
FiGS n-LPF	-35.6	-35.4	-34.9
FiGS nm-MT	-36.1	-35.2	-37.3

efficient in this context, the filter parameters can be set to the values given above (5 filters, $\alpha_0 = 99$ %) without risk relatively to the standard GS. Further improvements can be obtained by searching for the parameters leading to the lowest measurement errors, which is not computationally heavy once pseudo-inverses have been computed.

V. CONCLUSION

The filtering approach for Gerchberg-Saxton (GS) algorithm method for the two scan approach in phaseless spherical near-field has been reviewed. A filter yielding more accurate results in a stable way is proposed. Validations have been performed using simulations and experimental data and improvements in mean of several dB are achieved without additional cost. A next step is to further understand the relationship between the initialization methods, sampling size, parameters, filtering methods and the accuracy of the result. An adaptive approach for the tuning of the filter is of interest to further improve the results. Other phase retrieval procedures using spherical waves and based on convex optimization are also interesting options.

ACKNOWLEDGMENT

The authors thank Jerôme Sol and Benjamin Fuchs for the antenna measurements and prolific discussions on the subject.

REFERENCES

[1] J. Hald, J. Hansen, F. Jensen, and F. Larsen, *Spherical Near Field Antenna Measurements*. Peter Peregrinus, 1988.

[2] R. Moretta and R. Pierri, "Performance of phase retrieval via phaselift and quadratic inversion in circular scanning case," *IEEE Trans. on Antennas and Propag.*, vol. 67, no. 12, pp. 7528–7537, 2019.

[3] O. Breinbjerg and J. F. Álvarez, "Mathematical formulation of phase retrieval for phaseless spherical near-field antenna measurements with probe correction," in *URSI EMTS*, 2019.

[4] O. Bucci, G. D'Elia, G. Leone, and R. Pierri, "Far-field pattern determination from the near-field amplitude on two surfaces," *IEEE Trans. on Antennas and Propag.*, vol. 38, no. 11, pp. 1772–1779, 1990.

[5] A. Capozzoli, C. Curcio, G. D'Elia, and A. Liseno, "Phaseless antenna characterization by effective aperture field and data representations," *IEEE Trans. on Antennas and Propag.*, vol. 57, no. 1, pp. 215–230, 2009.

[6] F. Rodríguez Varela, J. Fernandez Álvarez, B. Galocha Iragüen, M. Sierra Castañer, and O. Breinbjerg, "Numerical and experimental investigation of phaseless spherical near-field antenna measurements," *IEEE Trans. on Antennas and Propag.*, vol. 69, no. 12, pp. 8830–8841, 2021.

[7] B. Fuchs, M. Mattes, S. Rondineau, and L. Le Coq, "Phaseless near-field antenna measurements from two surface scans — numerical and experimental investigations," *IEEE Trans. on Antennas and Propag.*, vol. 68, no. 3, pp. 2315–2322, 2020.

[8] F. Rodriguez Varela, J. Fernandez Álvarez, G. Belén Iragüen, M. Sierra Castañer, and O. Breinbjerg, "Combination of spherical and planar scanning for phaseless near-field antenna measurements," in *AMTA*, 2019, pp. 1–6.

[9] J. Fernandez Alvarez, M. Mattes, and O. Breinbjerg, "Phase retrieval for spherical near-field measurements using two antenna positions," in *AMTA, Florida*, 2021.

[10] N. Méziéres, L. Le Coq, and B. Fuchs, "Spherical phaseless antenna measurements experimental validation of a two-antenna-positions procedure," *IEEE Antennas Wirel. Propag. Lett.*, vol. 21, no. 4, pp. 813–817, 2022.

[11] A. Paulus, J. Knapp, and T. F. Eibert, "Phaseless near-field far-field transformation utilizing combinations of probe signals," *IEEE Trans. on Antennas and Propag.*, vol. 65, no. 10, pp. 5492–5502, 2017.

[12] S. Costanzo, G. Di Massa, and M. Migliore, "A novel hybrid approach for far-field characterization from near-field amplitude-only measurements on arbitrary scanning surfaces," *IEEE Trans. on Antennas and Propag.*, vol. 53, no. 6, pp. 1866–1874, 2005.

[13] R. Pierri and R. Moretta, "On data increasing in phase retrieval via quadratic inversion: Flattening manifold and local minima," *IEEE Trans. on Antennas and Propag.*, vol. 68, no. 12, pp. 8104–8113, 2020.

[14] C. Schmidt, S. Razavi, T. Eibert, and Y. Rahmat-Samii, "Phaseless spherical near-field antenna measurements for low and medium gain antennas," *Advances in Radio Science*, vol. 8, pp. 43–48, 09 2010.

[15] A. Bangun, C. Culotta-López, A. Behboodi, R. Mathar, and D. Heberling, "On phaseless spherical near-field antenna measurements," in *2019 13th EuCAP*, 2019, pp. 1–5.

[16] F. Jensen and A. Frandsen, "On the number of modes in spherical wave expansions," in *AMTA, Georgia*, 2004.

[17] J. R. Fienup, "Phase retrieval algorithms: a comparison," *Appl. Opt.*, vol. 21, no. 15, pp. 2758–2769, Aug 1982. [Online]. Available: https://opg.optica.org/ao/abstract.cfm?URI=ao-21-15-2758

[18] B. Fuchs, L. Le Coq, S. Rondineau, and M. D. Migliore, "Fast antenna far-field characterization via sparse spherical harmonic expansion," *IEEE Transactions on Antennas and Propagation*, vol. 65, no. 10, pp. 5503–5510, 2017.

[19] "Starlab 650MHz-18GHz," MVG, 2020, available at www.mvg-world.com/fr/products/antenna-measurement/multi-probe-systems/starlab.

[20] "Cst studio suite 2020," Dassault Systèmes, available at www.3ds.com/fr/produits-et-services/simulia/produits/cst-studio-suite/.

[21] D. Gonzalez-Ovejero, G. Minatti, E. Martini, G. Chattopadhyay, and S. Maci, "Shared aperture metasurface antennas for multibeam patterns," in *EUCAP*, 2017, pp. 3332–3335.